scientific reports

Check for updates

OPEN

Identification of the histologic transformation of follicular lymphoma using super-resolution microcirculation imaging

Ronghui Wang[1], Zhenhua Liu[1], Jipeng Yan[3], Siqi Hua[1], Zhiqian Wang[1], Zixun Yan[4], Xue Xie[2], Junnian Hao[2], Dan Zhou[1], Jianqiao Zhou[1], Weili Zhao[4]✉, Yuanyi Zheng[2]✉, Mengxing Tang[3] & Weiwei Zhan[1]✉

To investigate the ability of super-resolution microcirculation imaging in identifying high-risk histologic transformation (HT) regions, directing the targeted biopsies, and promising timely chemotherapy escalation and outcome improvement. Initially, a retrospective analysis (January 1, 2018–January 1, 2022) of indolent follicular lymphoma (FL) or aggressive diffuse large B cell lymphoma was conducted to identify imaging-based markers of distinguishing aggressive lymphoma from indolent lymphoma. Subsequently, the prospective research consecutively enrolled histologically confirmed FL patients between February 1, 2022, and May 31, 2024, to validate the diagnostic performance of these investigated indicators in differentiating aggressive transformed FL from FL. Diagnostic performance and the diagnostic consistency associated with time were assessed. A total of 132 participants were enrolled: 52 (age 53 years ± 14 [SD]; 34 males) in the retrospective cohort for development and 80 (age 55 years ± 12 [SD]; 34 males), including 10 initial biopsy-confirmed HT, in the prospective cohort for validation. Super-resolution microcirculation imaging demonstrated excellent sensitivity (100%; 95% CI 69.15–100%) and specificity (97.14%; 95% CI 90.06–99.65%) for HT detection, with minimal risk of missed lesions at initial diagnosis. This technique shows potential in early HT detection, facilitating timely chemotherapy escalation and reducing the need for repeat biopsies.

Keywords Follicular lymphoma, Ultrasound, Vascular remodelling

Follicular lymphoma (FL) is the most common indolent lymphoma, having a favorable prognosis (5-year survival rate of up to 90.6%). However, approximately 15–19% of patients eventually undergo histologic transformation (HT) to the more aggressive diffuse large B-cell lymphoma (DLBCL), with a follow-up of 6–8 years[1], at an estimated annual rate of 2–3%[2]. This transformation significantly worsens outcomes[3–5], but there are no reliable methods to accurately predict and preempt such transformed follicular lymphoma (tFL). Moreover, prophylactic use of chemotherapy can lead to poorer outcomes in patients subsequently experiencing HT[6–8]. Therefore, early detection of HT is critical for timely chemotherapy escalation and improving patient outcomes.

Currently, HT confirmation depends on diagnostic biopsy, but the spatial heterogeneity of FL frequently necessitates multiple-site biopsies to detect occult transformation[9–11]. While 18-fluorodeoxyglucose-positron emission tomography (FDG-PET) may provide a reference biopsy site, its applicability remains controversial. Previous studies found that FDG standardized uptake values (SUVs) were higher in aggressive lymphoma[12], with values exceeding 10 to 13 to differentiate aggressive lymphoma from indolent lymphoma[13,14]. However, a study focused on HT indicated that SUVs at biopsy-proven HT sites ranged from 3 to 38[15]. This overlap between indolent and aggressive lymphomas impedes FDG-PET in confirming HT[10]. In addition, the high cost

[1]Department of Ultrasound, Ruijin Hospital, Shanghai Jiao Tong University School of Medicine, Shanghai 200025, People's Republic of China. [2]Department of Ultrasound, Shanghai Sixth People's Hospital Affiliated to Shanghai Jiao Tong University School of Medicine, 600 Yishan Road, Xuhui District, Shanghai 200233, People's Republic of China. [3]Ultrasound Lab for Imaging and Sensing, Department of Bioengineering, Imperial College London, London SW7 2AZ, UK. [4]Shanghai Institute of Hematology, State Key Laboratory of Medical Genomics, National Research Center for Translational Medicine at Shanghai, Ruijin Hospital, Shanghai Jiao Tong University School of Medicine, Shanghai 200025, People's Republic of China. ✉email: zhao.weili@yahoo.com; zhengyuanyi@163.com; shanghairuijinus@163.com

of scanning and the increased radiation exposure risk[16] of PET limit its routine application for monitoring HT. Consequently, a non-ionizing, cost-effective, and high-specific imaging technique is urgently needed to identify high-risk HT regions and guide targeted biopsy.

Microenvironment research has elucidated microvascular roles in FL progression, such as germinal center effacement and the involvement of tumor-associated macrophages (TAMs)[17–19], promoting neovascularization and vascular remodeling via secreting vascular endothelial growth factors[20,21]. The absence of high endothelial veins is another feature associated with aggressive lymphoma[22]. These findings suggest microvascular changes, including microvascular density and vascular remodeling, may be valuable indicators for HT detection.

In this context, this study introduced super-resolution microcirculation imaging, including maximum intensity projection (MIP) and ultrasound localization microscopy (ULM) for HT detection. These advanced imaging modalities provide insights into vascular architecture, with MIP effectively capturing perfusion dynamics by aggregating each CEUS frame with its predecessor[23] and ULM visualizing high-resolution microvascular networks by localizing and tracking microbubbles and determining their spatial distribution[24]. This study aimed to evaluate the diagnostic efficacy of super-resolution microcirculation imaging in identifying high-risk HT regions, improving biopsy targeting, avoiding missing the HT diagnosis, and minimizing unnecessary repeat biopsies.

Methods

Participants and study design

This study includes a retrospective phase for development and a prospective phase for validation. Ethical approval was granted by the Hospital Ethics Committee in concordance with the Declaration of Helsinki, with written informed consent from all participants. The Clinical Trial Registry Number is ChiCTR2100048361. Figure 1 details the patient enrollment process.

A retrospective study (January 1, 2018–January 1, 2022) consecutively enrolled histologically confirmed untreated FL or DLBCL patients (aged ≥ 18) to investigate potential indicators in differentiating indolent FL with aggressive DLBCL by analyzing US, CEUS, and MIP images. All the enrolled patients had comprehensive US images of biopsy lymph nodes, while those without enlarged peripheral lymph nodes or with surgically removed lesions were excluded. For mean vascular density analysis, participants were stratified by frame rate, high (30 fps) or low (10 fps), to calculate peak intensities of CEUS, a quantitative parameter reflecting the mean vascular density. Only high-framerate recordings with superior quality were selected for MIP generation, as they better capture centrifugal enhancement trajectory (Supplementary Movies S1-S2).

The prospective study (February 1, 2022–May 31, 2024) consecutively enrolled histologically confirmed untreated FL admission patients (aged ≥ 18) to test the diagnostic performance of these investigated indicators in HT detection. Exclusion criteria mirrored those in the retrospective study. The admission patients were identified as potentially meeting the Group d'Etudes des Lymphomes Folliculaires (GELF) criteria[25], necessitating

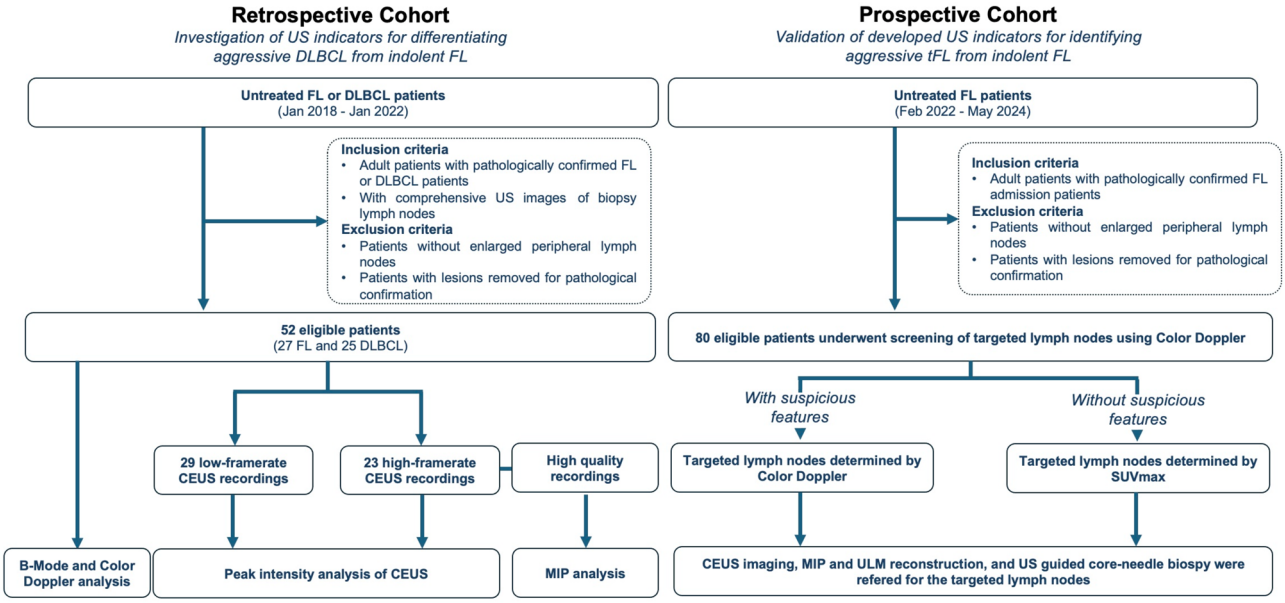

Fig. 1. Patient enrollment flowchart. The retrospective cohort enrolled 52 eligible patients with follicular lymphoma (FL) or diffuse large B cell lymphoma (DLBCL) to investigate imaging indicators for distinguishing aggressive DLBCL from indolent FL. Following this, 80 FL patients were recruited in the prospective cohort to validate the diagnostic performance of these indicators in differentiating aggressive transformed follicular lymphoma (tFL) from indolent FL. *US* ultrasound, *B-mode* brightness modes, *CEUS* contrast-enhanced ultrasound, *MIP* maximum intensity projection, *ULM* ultrasound localization microscopy, *SUVmax* maximum standardized uptake.

immunotherapy or immunochemotherapy. Leveraging the diagnostic potential of Color Doppler imaging in the retrospective study and the previous SUVmax data for HT detection[12–14], the targeted peripheral lymph nodes were selected by the Color Doppler and SUVmax. The specific screening criteria were as follows: Initially, all peripheral lymph nodes of the enrolled patients were evaluated using Color Doppler scanning. For patients whose lymph nodes exhibited suspicious features on Color Doppler, preference was given to targeting these specific nodes. In cases where no suspicious features were observed, the peripheral lymph node with the highest SUVmax was selected as the targeted lymph node. All the targeted lymph nodes were subsequently referred for CEUS examination, MIP and ULM image generation, and US-guided core-needle biopsy. Imaging procedure and parameter settings were in Supplemental Methods S1 and Table S1. The generation of MIP and ULM images are presented in Supplemental Methods S2 and S3, respectively. The schematic of MIP generation is provided in Supplemental Figure S1.

Pathologic evaluation

The time interval between imaging scanning and core-needle biopsy is less than 7 days. All the images were not available to pathologic reviewers. The pathologic classification is based on the 2016 World Health Organization Classification[26]. Initial pathological diagnosis of the biopsy site at admission was documented alongside the final pathologic diagnosis post the six cycles of therapy. The final diagnosis was determined by pathologic evaluation of biopsies obtained during the six treatment cycles. Patients with biopsy-confirmed HT during this period were classified as HT, while those without evidence of disease progression or biopsy-confirmed HT were categorized as FL.

Image interpretation

Two radiologists with 10 (RH. W.) and 14 (ZH. L.) years of superficial ultrasound experience independently reviewed ultrasound images, with a third radiologist with 14 years (ZQ. W.) of experience in superficial ultrasound resolving discrepancies. All reviewers were blinded to histopathological results.

On brightness-mode (B-mode) ultrasound, the visibility of a hyperechogenic hilum indicates whether the hilum is present. Color Doppler assessed vessel structure and flow grading, defining "hilar flow" as a central vessel aligned with the lymph node's long axis or radial vessels from one point and "mixed flow" as multiple radial sources. Blood flow was graded as minimal (no or spot color), moderate (fewer than three confluent vessels), or abundant (more than three confluent vessels).

Using CEUS videos, time-intensity curve analysis software (Mindary, China) quantitative calculated lymph nodes' peak intensities. The perfusion patterns of centrifugal enhancement (contrast agents filling the center and dispersing outward) and starry-sky enhancement (simultaneous enhancement of multiple points) were used to evaluate the perfusion dynamics.

MIP-ULM analysis identified "firework enhancement" as a single enhanced dot or trunk at the hilum expanding radially, whereas "mixed enhancement" includes starry-sky or centrifugal patterns from multiple sources. In ULM, red color coding indicates flow toward the transducer, and blue indicates flow away. The ULM angle map displays microvessel orientations, with a pie chart correlating colors to directional data.

Different indicators for HT identification

This prospective cohort of 80 patients was enrolled to evaluate the diagnostic performance of LDH level, Color Doppler, CEUS, and super-resolution microcirculation imaging in HT detection. Among these, 55 who underwent PET/CT at our institution had additional diagnostic efficacy evaluation, including the above methods and SUVmax, using a threshold of > 10 for HT identification.

Temporal variations of diverse indicators in diagnostic classification

Initial pathological diagnosis of the biopsy site at admission was documented alongside the final pathologic diagnosis post the six cycles of therapy with obinutuzumab-lenalidomide (GR), obinutuzumab-bendamustine (GB), obinutuzumab -based cyclophosphamide, doxorubicin, vincristine, and prednisone (CHOP) or rituximab-based CHOP regimen to assess the predictive capabilities of different indicators.

Outcomes

Following six treatment cycles, the endpoint was assessed by PET-CT, following the Lugano 2014 criteria[27]. The status of the mediastinum and retroperitoneal lesions before and after the treatment was determined based on PET/CT reports.

Statistical analysis

To investigate the diagnostic efficiency, we used PASS software (NCSS, USA) with a two-sided significance level of 0.05, 80% power, an estimated prevalence of 0.15, and target sensitivity and specificity of 98 and 95%, respectively, the software calculated a sample size of 73 participants with 11 HT. Statistical tests included Pearson's Chi-Square for categorical comparisons of US images in FL and DLBCL, Mann Whitney U test for ordinal and continuous data, and Fisher's exact test for categorical variables. McNemar test assessed diagnostic performance discrepancies among various methods. Diagnostic performance was calculated using the histopathology of the biopsy site as the gold standard. All analyses were performed using IBM SPSS version 23.

Results

Retrospective study

Patient characteristics

Between January 1, 2018, and January 1, 2022, we retrospectively enrolled 52 untreated patients aged ≥ 18 with biopsied lymph nodes, including 27 FL and 25 DLBCL patients. Baseline characteristics between FL and DLBCL patients are shown in Table 1. Of the 52 patients, only 14 were selected for MIP generation due to the limitation of image quality. As demonstrated in Supplemental Movies S1 and S2, capturing the centrifugal enhancement trajectory necessitates high frame-rate imaging, which has only recently become widely available.

Conventional US

Typical blood flow grading images are illustrated in Fig. 2A. A higher proportion (76%, 19/25) of DLBCL patients exhibited hilum absent compared to FL patients (44.44%, 12/27) ($\chi2 = 5.37$, $P = 0.02$) in Fig. 2B. Additionally, the hilar flow was more frequent in FL (88.89%, 24/27) than in DLBCL (16%, 4/25) ($\chi2 = 27.75$, $P < 0.001$) in Fig. 2C. Conversely, blood flow grading failed to show a significant difference or correlation between FL and DLBCL ($\chi2 = 3.10$, $P = 0.21$; Cramer's value = 0.24, $P = 0.21$) in Fig. 2D. These findings indicated that the mixed flow was considered a suspicious Color Doppler indicator for screening the target suspicious peripheral lymph nodes for further evaluation.

CEUS

The median peak intensities from low-framerate CEUS for FL and DLBCL patients were 108.0 (IQR 91.0–127.0) and 117.0 (IQR 83.5–134.8), respectively, and from high-framerate CEUS were 52.0 (IQR 39.5–82.0) for FL and 43.0 (IQR, 31.0–75.0) for DLBCL (Fig. 2E–H). Unluckily, neither high- nor low-framerate CEUS revealed significant differences between FL and DLBCL. The *P*-values for high- and low-framerate CEUS were 0.37 and 0.75, respectively. Thus, the peak intensity of CEUS, a quantitative parameter reflecting the mean vascular density (MVD)[28,29], did not effectively differentiate between FL and DLBCL in our cohort.

MIP

MIP images from high-framerate CEUS recordings in 14 patients showed distinct patterns: DLBCL patients exhibited a "starry-sky" enhancement with multiple scattered enhanced dots growing in number over time, whereas FL demonstrated a "firework" enhancement with one enhanced dot at the hilum radially exploded over time in Fig. 2I. These findings suggest that vascular structural changes, rather than density increases, may contribute to HT.

Characteristics (n = 52)	FL-indolent or DLBCL-aggressive Lymphoma		*P* value
	FL (n = 27)	DLBCL (n = 25)	
Age	49 ± 12	57 ± 15	0.035
Gender			
Male	18 (66.7%)	16 (64%)	1.000
Female	9 (33.3%)	9 (36%)	
BM			
Positive	14 (51.9%)	4 (16%)	0.009*
Negative	13 (48.1%)	21 (84%)	
LDH			0.019*
Normal	22 (81.5%)	12 (48%)	
> ULN	5 (18.5%)	13 (52%)	
Hb			
Low(< 120 g/L)	7 (25.9%)	5 (20%)	0.746
Normal/High	20 (74.1%)	20 (80%)	
Max size			
< 6 cm	21 (77.8%)	20 (80%)	1.000
≥ 6 cm	6 (22.2%)	5 (20%)	
β2-Microglobulin			1.000
Normal	19 (70.4%)	17 (68%)	
> ULN	8 (29.6%)	8 (32%)	

Table 1. Baseline characteristics of patients with FL and DLBCL in the retrospective study. *Hb* haemoglobin, *LDH* lactate dehydrogenase, *BM* bone marrow, *ULN* upper limit of normal, *FL* follicular lymphoma, *DLBCL* diffuse large B cell lymphoma. * $P < 0.05$ was considered indicative of a statistically significant difference.

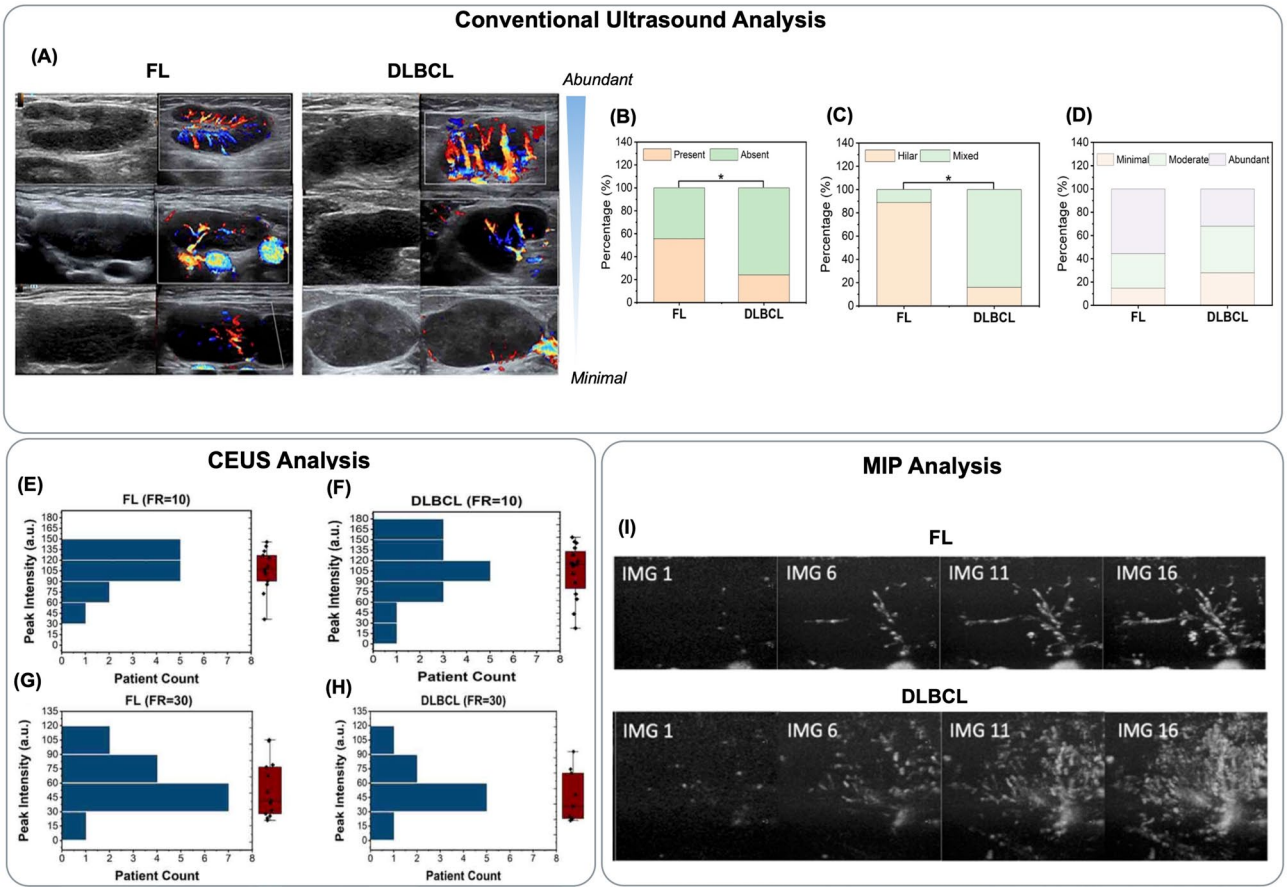

Fig. 2. Imaging-based indicators of conventional ultrasound, contrast-enhanced ultrasound (CEUS), and maximum intensity projection (MIP) in the retrospective cohort for differentiating indolent and aggressive Lymphoma. (**A**) Representative Color Doppler images of follicular lymphoma (FL) (left) and diffuse large B cell lymphoma (DLBCL) (right) showcasing various levels of blood flow: abundant (top), moderate (middle), and minimal (bottom). Bar graphs depicted the proportion of FL and DLBCL patients (**B**) with or without hilum on brightness-modes (B-mode) ultrasound, **(C)** presence or absence of hilar flow on Color Doppler, and (**D**) different grades of blood flow (minimal, moderate, abundant) on Color Doppler. Box plots illustrating the distribution and probability of peak intensities of the biopsied lymph nodes from CEUS analysis in FL and DLBCL patients. Data is separated by framerate (FR): (**E**, **F**) low FR (10 frames per second, fps), (**G**, **H**) high FR (30 fps). (**I**) Representative MIP images of FL (top row) and DLBCL (bottom row) lymph nodes showcasing distinct enhancement patterns. FL showed a "firework" pattern, while DLBCL exhibited a "starry sky" pattern. * $P < 0.05$ was considered indicative of a statistically significant difference.

Prospective study

Patient characteristics

Between February 1, 2022, and May 31, 2024, 80 untreated patients with histologically confirmed FL admission patients were enrolled. In this cohort, the mean age of FL and tFL patients was 54 years ± 12 [SD] and 58 years ± 13 [SD], respectively ($P = 0.312$). Table 2 presents the baseline characteristics of FL and tFL patients. Most enrolled admission patients (83.75%, 67/80) met the GELF criteria, necessitating immunotherapy or immunochemotherapy. 12.5% (10/80) admission patients were assigned to watch and wait.

Typical images

Figure 3A showcases images of FL patients, illustrating typical findings across different imaging modalities: hilar flow on Color Doppler, centrifugal enhancement on CEUS, firework enhancement on MIP, and classic hilar vessel on ULM, respectively. In HT patients, MIP images exhibited two subtypes of "mixed enhancement": starry-sky enhancement (Fig. 3B) and centrifugal enhancement from multiple sources (Fig. 3C). ULM images for the starry-sky subtype displayed chaotic vessel orientations (Fig. 3D), while the other subtype showed multi-source flow patterns (Fig. 3E).

Diagnostic performance of different indicators for HT identification

Indicators from various imaging and blood test techniques were assessed for their diagnostic effectiveness in identifying HT, including mixed flow on Color Doppler, starry-sky enhancement on CEUS, and mixed enhancement on MIP and ULM, as well as elevated LDH levels and SUVmax > 10. The detailed diagnostic metrics

Characteristics (n = 80)	With or without histologic transformation		*P* Value
	FL (n = 70)	tFL (n = 10)	
Age	54 ± 12	58 ± 13	0.312
Gender			0.310
Male	28 (40%)	6 (60%)	
Female	42 (60%)	4(40%)	
BM			0.172
Positive	34 (48.6%)	2 (20%)	
Negative	36 (51.4%)	8(80%)	
LDH			0.410
Normal	57 (81.4%)	7 (70%)	
> ULN	13 (18.6%)	3 (30%)	
Hb			1.000
Low(< 120 g/L)	19 (27.1%)	2 (20%)	
Normal/High	51 (72.9%)	8 (80%)	
Max size			0.481
< 6 cm	44 (62.9%)	8 (80%)	
≥ 6 cm	26 (37.1%)	2 (20%)	
β2-Microglobulin			0.747
Normal	39 (55.7%)	5 (50%)	
> ULN	31 (44.3%)	5 (50%)	
FLIPI2			0.920
Low (0–1)	27 (38.6%)	4 (40%)	
Intermediate (2)	21 (30%)	3 (30%)	
High (≥ 3)	22 (31.4%)	3 (30%)	

Table 2. Baseline characteristics of patients with FL and tFL. *Hb* haemoglobin, *LDH* lactate dehydrogenase, *BM* bone marrow, *ULN* upper limit of normal, *FLIPI2* Follicular Lymphoma International Prognostic Index 2, *FL* follicular lymphoma, *tFL* transformed follicular lymphoma. * $P < 0.05$ was considered indicative of a statistically significant difference.

for each indicator are summarized in Tables 3 and 4. The combined use of MIP and ULM achieved promising diagnostic accuracy (97.5%; 95%CI 91.26–99.7%) for HT identification. Although LDH levels showed high specificity, their sensitivity was limited. Similarly, SUVmax demonstrated high sensitivity but limited specificity.

Notably, three tFL cases were misdiagnosed by CEUS. Of these, two can be detected via Doppler's mixed flow, while one case escaped detection by both Doppler and CEUS detection (Supplementary Fig. S2A and Movie S3). However, this undetected case was successfully identified by super-resolution microcirculation imaging (Supplemental Fig. S2B,C). Among eight FL misclassifications on Color Doppler, 6 out of 8 were misdiagnosed due to the angle dependence limitation of Color Doppler: Blood flow perpendicular to the ultrasound beam, undetectable in Doppler but visible with ULM (Supplemental Fig. S3A,B). Although the microcirculation imaging showed promising diagnostic performance, it did not show any statistical significance among these techniques with this limited sample size.

Temporal variations in diagnostic classification

The predictive ability of LDH and super-resolution microcirculation imaging for HT was assessed over six treatment cycles (Fig. 4A,B). Combined MIP-ULM indicators showed strong concordance with pathological diagnoses of the biopsy site and final diagnosis after six cycles of treatment, with 95.59% (65/68) firework enhancement and 91.67% (11/12) mixed enhancement matching the final diagnosis of FL and HT, respectively. Three unmatched FL patients were confirmed as HT via biopsy of the new lesions in the liver, forearm, and stomach, absent on baseline PET scans.

In a subgroup of 55 patients with PET scans, Fig. 4C demonstrates that SUVmax < 10 was linked to a lower HT rate, but distinguishing tFL from FL became challenging at SUVmax values > 10. On the contrary, MIP-ULM consistently excelled in distinguishing tFL from FL regardless of cohort size (Fig. 4B,D). Considering SUVmax > 10 as the diagnostic threshold of PET for HT detection, the new imaging method showed a significantly lower false-positive rate (1.54%, 1/65) compared to PET/CT (39.53%, 17/43), highlighting its potential to reduce unnecessary repeat biopsies via guiding biopsies the high-risk HT regions.

Outcomes

As shown in Fig. 4E, follow-up after six treatment cycles revealed that among 46 FL patients receiving GR or GB regimens, 84.78% (39/46) achieved complete response (CR), 6.52% (3/46) had partial response (PR), and 8.7% (4/46) experienced disease progression (PD). Of the four PD patients, three had histologically confirmed new

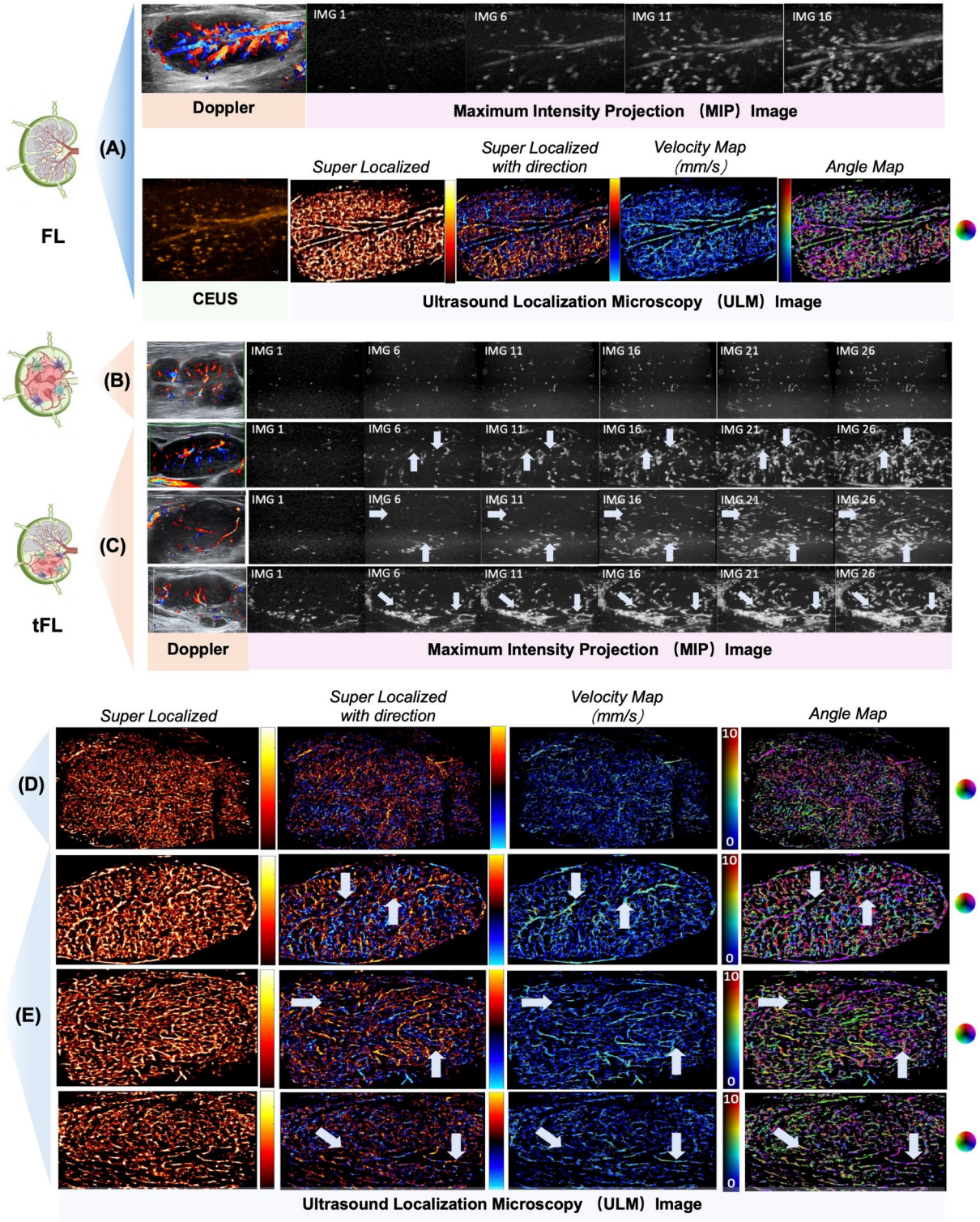

Fig. 3. Distinct vascular features of follicular lymphoma (FL) and transformed follicular lymphoma (tFL). (**A**) Representative images of an FL patient demonstrated typical findings: hilar flow on Color Doppler, centrifugal enhancement on contrast-enhanced ultrasound (CEUS), and firework enhancement patterns on maximum intensity projection (MIP) with classic hilar vessels on ultrasound localization microscopy (ULM). In contrast, tFL presents two characteristic mixed enhancement patterns on MIP: (**B**) a starry-sky pattern characterized by multiple scattered enhancing dots growing in number over time and (**C**) two or more firework patterns originating from multiple sources. These patterns are further visualized on ULM with (**D**) chaotic vessels from multiple directions in the "starry-sky" subtype and (**E**) vessels originating from multiple sources. Arrows indicated distinct vessel origins.

Characteristics (n = 80)	Sensitivity	Specificity	PPV	NPV	Accuracy
LDH	30 (6.67–65.25)	81.43 (70.34–89.72)	18.75 (7.36–40.13)	89.06 (84.24–92.54)	75 (64.06–84.01)
Color doppler	80 (44.39–97.48)	88.57 (78.72–94.94)	50 (32.69–67.31)	96.88 (89.95–99.08)	87.5 (78.21–93.84)
CEUS	70 (34.76–93.33)	88.57 (78.72–94.94)	46.67 (28.87–65.35)	95.39 (88.88–98.16)	86.25(76.73–92.93)
MIP and ULM	100 (69.15–100)	97.14 (90.06–99.65)	83.33 (56.06–95.15)	100 (94.72–100)	97.5 (91.26–99.7)

Table 3. Diagnostic performance of LDH, Color Doppler, CEUS, and combination of MIP and ULM. Data are percentages with a 95% confidence interval in parentheses. *PPV* positive predict value, *NPV* negative predict value, *CEUS* contrast-enhanced ultrasound, *MIP* maximum intensity projection, *ULM* ultrasound localization microscopy, *LDH* lactate dehydrogenase.

Characteristics (n = 55)	Sensitivity	Specificity	PPV	NPV	Accuracy
LDH	25 (3.19–65.09)	80.85 (66.74–90.85)	18.18 (5.52–45.82)	86.36 (80.57–90.63)	72.73 (59.04–83.86)
SUVmax	100 (63.06–100)	57.45 (42.18–71.74)	28.57 (22.3–35.8)	100 (87.23–100)	63.64 (49.56–76.19)
Color doppler	87.5 (47.35–99.68)	89.36 (76.90–96.45)	58.33 (36.99–76.95)	97.67 (87.01–99.62)	89.09 (77.75–95.89)
CEUS	75 (34.91–96.82)	87.23 (74.26–95.17)	50 (29.99–70.01)	95.35 (86–98.56)	85.46 (73.34–93.51)
MIP and ULM	100 (63.06–100)	97.87 (88.71–99.95)	88.89 (53.5–98.23)	100 (92.29–100)	98.18 (90.28–99.95)

Table 4. Diagnostic performance of LDH, SUVmax, Color Doppler, CEUS, and a combination of MIP and ULM: Subgroup analysis of patients with PET scan in our institution. Data are percentages with a 95% confidence interval in parentheses. *PPV* positive predict value, *NPV* negative predict value, *CEUS* contrast-enhanced ultrasound, *MIP* maximum intensity projection, *ULM* ultrasound localization microscopy, *LDH* lactate dehydrogenase, *SUVmax* maximum standardized uptake value, *PET* positron emission tomography.

HT lesions, while one showed residual high SUV lesions confirmed as FL via re-biopsy of the residual lesion. Figure 4F highlights that only 3 out of 67 received immunochemotherapy patients had residual lesions with SUVmax > 10, while most had either resolved lesions or low SUV residual lesions, suggesting tissue sampling from deep locations is often unnecessary without definitive signs of HT.

Discussion

Early HT detection in FL is crucial for determining prognosis and timely chemotherapy escalation. HT confirmation relies on biopsies, which require robust imaging indicators to identify and target the biopsy of the high-risk HT regions. Currently, FDG-PET-based HT suspicious criteria may provide a reference biopsy site, but a 39.53% false-positive rate of PET-CT in our cohort suggested that it might hardly avoid the unnecessary repeat biopsy and complicates biopsy-site decision-making of de novo FL patients with multiple high SUVmax lesions (generally > 10). Moreover, Studies on FL progression further highlight the possibility of occult HT that may be missed with current diagnostic approaches[8,30]. Given these challenges, this study introduced super-resolution ultrasound microcirculation imaging, including MIP and ULM demonstrated high specificity (97.14%; 95%CI 90.06–99.65%) and sensitivity (100%; 95%CI 69.15–100%) with a remarkable low false-positive rate (1.54%). Meanwhile, MIP-ULM showed high concordance with the biopsy site and final diagnoses, demonstrating that almost all the HT patients were captured by MIP-ULM. For the three missed HT patients, HT confirmation was via biopsy of the new lesions in the liver, forearm, and stomach, which did not appear on the baseline PET scan. Although the 18.75% (15/80) HT rate observed in our cohort exceeds the generally accepted annual transformation risk of 2–3%, the higher incidence, combined with the 84.78% (39/46) CR rate, and 6.52% (3/46) PR rate, supported the efficacy of our technique, which may help detect occult transformation before treatment. Additionally, the high HT rate in our cohort also aligns with the reported 15–19% incidence of HT after 6–8 years of follow-up[1].

Notably, our findings reinforce the hypothesis that vascular remodeling, rather than density alone, is a more reliable indicator for HT detection in FL. Prior research has shown that tumor-associated macrophages (TAMs), particularly the M2 subtype, contribute to vascular remodeling by secreting vascular endothelial growth factors[18,20,21], resulting in a more tortuous vascular architecture[31,32]. Consistent with this, our results revealed patterns such as mixed flow on Color Doppler, starry-sky enhancement on CEUS, and mixed enhancement on MIP-ULM. These observations align with single-cell atlas data suggesting stromal remodeling in HT patients[33]. Together, these findings underscore the significance of vascular structural changes in HT assessment and highlight the value of super-resolution microcirculation imaging in providing a more nuanced change of microvascular structure without the angle dependence limitation of Color Doppler[34]. Meanwhile, MIP-ULM showed greater benefit for HT detection than LDH and PET, which are currently used in clinical practice but are limited in offering a precise anatomical site of HT or low specificity, leading to unnecessary repeat biopsies.

Although the results are encouraging, this study had limitations. Firstly, ultrasound faces challenges in certain anatomical locations, particularly the mediastinum and retroperitoneum. Notably, deep anatomical locations pose significant challenges for tissue sampling. In the absence of definitive evidence of HT, these areas are not prioritized for biopsy. Ultrasound's efficacy in evaluating peripheral lymph nodes presents a viable alternative for

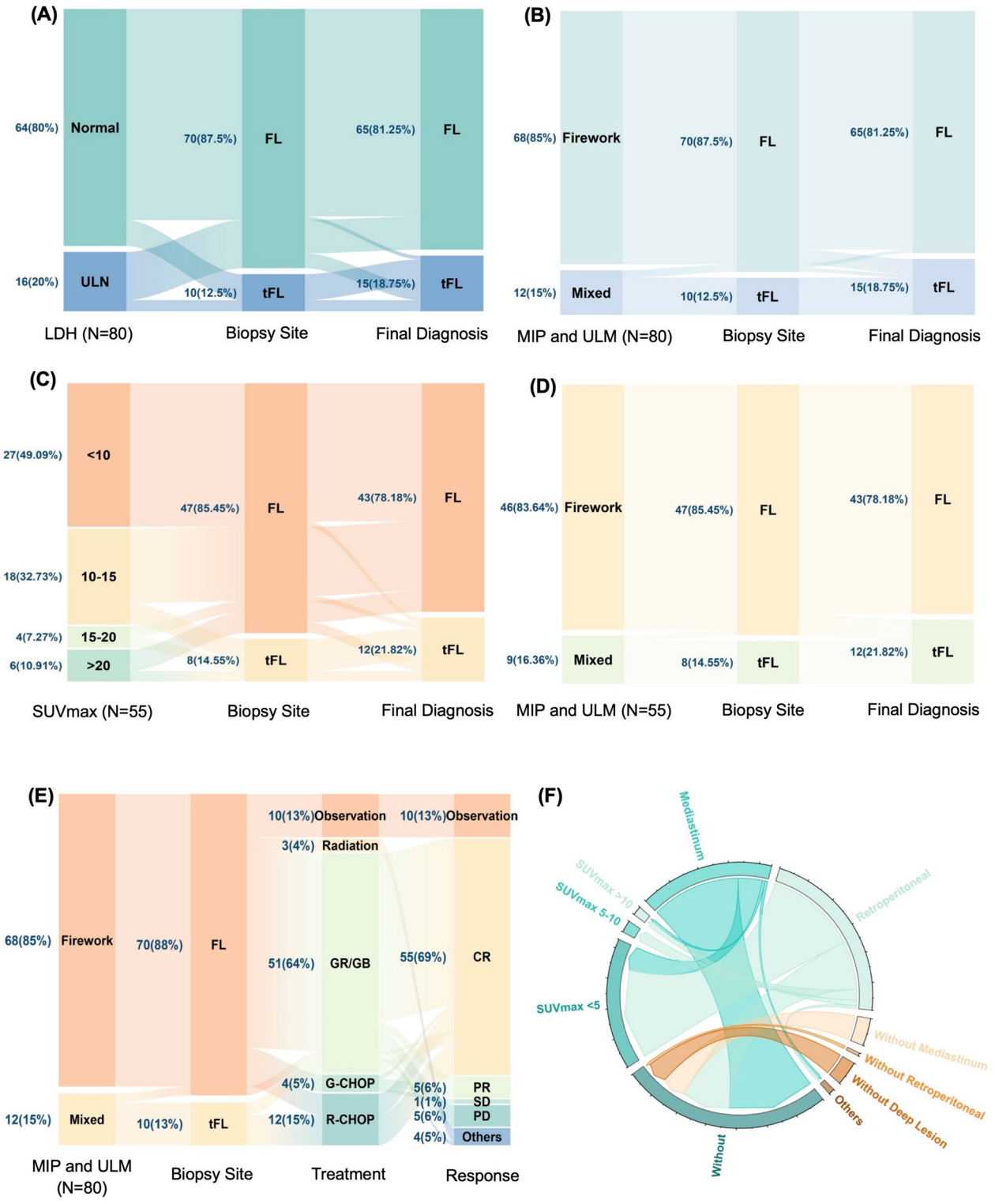

Fig. 4. Diagnostic and treatment evaluation. (**A**–**D**) Sankey diagrams visualized the diagnostic classification journey and the predictive ability of lactate dehydrogenase (LDH), maximum standardized uptake (SUVmax), and maximum intensity projection-ultrasound localization microscopy (MIP-ULM) techniques. (**E**) Response evaluation following six cycles of the initial treatment regimen. (**F**) A chord diagram represented the lesion status at deep locations before and after treatment, with arrows pointing to the lesion status at the end of the treatment. The "Others" classification represents patients lost to follow-up in the study. *FL* follicular lymphoma, *tFL* transformed follicular lymphoma, *ULN* upper limit of normal, *GR/GB* obinutuzumab plus lenalidomide or obinutuzumab plus bendamustine, *G-CHOP* obinutuzumab-based cyclophosphamide, doxorubicin, vincristine, and prednisone, *R-CHOP* rituximab-based cyclophosphamide, doxorubicin, vincristine, and prednisone, *CR* completely response, *PR* partial response, *SD* stable disease, *PD* progressive disease.

detecting HT in peripheral tissues, potentially reducing the need for high-risk deep-tissue biopsies. Considering almost no HT patients were missed in our cohort, weighing the pros and cons, we recommend utilizing MIP and ULM for screening peripheral lymph nodes during the initial evaluation. In cases where no evidence of HT is found in the peripheral lymph nodes, a biopsy should be performed on regions exhibiting high SUVmax values (generally > 10). Secondly, the sample size of enrolled patients in the prospective study was insufficient to compare the diagnostic performance among different techniques. Thirdly, findings from a single center may hinder the generalization of our results.

In conclusion, this pilot study demonstrated that super-resolution microcirculation imaging-MIP and ULM is a cost-effective and promising alternative, but requires further validation methods for HT detection in FL. This innovative technique enhanced diagnostic precision, reducing the risk of missing HT and avoiding unnecessary repeat invasive procedures. However, considering the limitations of US in evaluating deep-seated lesions, PET-CT-guided biopsy was still recommended to supplement cases where no HT evidence was found in peripheral lymph nodes. Future research should prioritize the development of non-contrast microvascular imaging techniques for HT detection, comparing this approach with existing imaging modalities and investigating its integration into routine clinical workflows to optimize the management of FL and improve patient outcomes.

Data availability

The datasets generated and analyzed during the current study are available from the corresponding author on reasonable request. The software for ULM image generation was available on (https://github.com/JipengYan1995/SRUSSoftware).

Received: 19 January 2025; Accepted: 7 May 2025
Published online: 13 May 2025

References

1. Wagner-Johnston, N. D. et al. Outcomes of transformed follicular lymphoma in the modern era: a report from the National LymphoCare Study (NLCS). *Blood* **126**, 851–857 (2015).
2. Federico, M. et al. Rituximab and the risk of transformation of follicular lymphoma: a retrospective pooled analysis. *Lancet Haematol.* **5**, e359–e367 (2018).
3. Bastion, Y. et al. Incidence, predictive factors, and outcome of lymphoma transformation in follicular lymphoma patients. *J. Clin. Oncol.* **15**, 1587–1594 (1997).
4. Sarkozy, C. et al. Risk factors and outcomes for patients with follicular lymphoma who had histologic transformation after response to first-line immunochemotherapy in the PRIMA trial. *J. Clin. Oncol.* **34**, 2575–2582 (2016).
5. Kridel, R., Sehn, L. H. & Gascoyne, R. D. Can histologic transformation of follicular lymphoma be predicted and prevented?. *Blood* **130**, 258–266 (2017).
6. Link, B. K. et al. Rates and outcomes of follicular lymphoma transformation in the immunochemotherapy era: a report from the University of Iowa/Mayo Clinic Specialized Program of Research Excellence Molecular Epidemiology Resource. *J. Clin. Oncol.* **31**, 3272 (2013).
7. Ban-Hoefen, M. et al. Transformed non-Hodgkin lymphoma in the rituximab era: analysis of the NCCN outcomes database. *Br. J. Haematol.* **163**, 487–495 (2013).
8. Smith, S. Transformed lymphoma: what should I do now?. *Hematol. Am. Soc. Hematol. Educ. Program* **4**, 306–311 (2020).
9. Alcoceba, M., Alonso-Álvarez, S., García-Álvarez, M., Martín, A. & Caballero, M. D. Unmet needs in histological transformation of follicular lymphoma: a clinical and biological review. *Ann. Lymphoma* **1**, 11 (2017).
10. Casulo, C., Burack, W. R. & Friedberg, J. W. Transformed follicular non-Hodgkin lymphoma. *Blood* **125**, 40–47 (2015).
11. Mikhaeel, N. G. Hotter is not more aggressive: baseline SUVmax in FL. *Blood* **135**, 1191–1192 (2020).
12. Karam, M. et al. Role of fluorine-18 fluoro-deoxyglucose positron emission tomography scan in the evaluation and follow-up of patients with low-grade lymphomas. *Cancer* **107**, 175–183 (2006).
13. Schöder, H. et al. Intensity of 18fluorodeoxyglucose uptake in positron emission tomography distinguishes between indolent and aggressive non-Hodgkin's lymphoma. *J. Clin. Oncol.* **23**, 4643–4651 (2005).
14. Ngeow, J. Y. Y. et al. High SUV uptake on FDG–PET/CT predicts for an aggressive B-cell lymphoma in a prospective study of primary FDG–PET/CT staging in lymphoma. *Ann. Oncol.* **20**, 1543–1547 (2009).
15. Noy, A. et al. The majority of transformed lymphomas have high standardized uptake values (SUVs) on positron emission tomography (PET) scanning similar to diffuse large B-cell lymphoma (DLBCL). *Ann. Oncol.* **20**, 508–512 (2009).
16. de Basea, Bosch et al. Risk of hematological malignancies from CT radiation exposure in children, adolescents, and young adults. *Nat. Med.* **29**, 3111–3119 (2023).
17. Shiozawa, E. et al. Disappearance of CD21-positive follicular dendritic cells preceding the transformation of follicular lymphoma: immunohistological study of the transformation using CD21, p53, Ki-67, and P-glycoprotein. *Pathol. Res. Pract.* **199**, 293–302 (2003).
18. de Jong, D. & Fest, T. The microenvironment in follicular lymphoma. *Best Pract. Res. Clin. Haematol.* **24**, 135–146 (2011).
19. Fowler, N. H. *Follicular Lymphoma: Current Management and Novel Approaches* (Springer Nature, 2019).
20. Blanco, M., Collazo-Lorduy, A., Yanguas-Casás, N., Calvo, V. & Provencio, M. Unveiling the Role of the Tumor Microenvironment in the Treatment of Follicular Lymphoma. *Cancers (Basel)* **14**, 2158 (2022).
21. Chen, Y. et al. Tumor-associated macrophages: an accomplice in solid tumor progression. *J. Biomed. Sci.* **26**, 78 (2019).
22. Menzel, L. et al. Lymphocyte access to lymphoma is impaired by high endothelial venule regression. *Cell Rep.* **37**, 109878 (2021).
23. Rafailidis, V., Huang, D. Y., Yusuf, G. T. & Sidhu, P. S. General principles and overview of vascular contrast-enhanced ultrasonography. *Ultrasonography.* **39**, 22–42 (2020).
24. Cox, B. & Beard, P. Super-resolution ultrasound. *Nature* **527**, 451–452 (2015).
25. Brice, P. et al. Comparison in low-tumor-burden follicular lymphomas between an initial no-treatment policy, prednimustine, or interferon alfa: a randomized study from the Groupe d'Etude des Lymphomes Folliculaires. Groupe d'Etude des Lymphomes de l'Adulte. *J. Clin. Oncol.* **15**, 1110–1117 (1997).
26. Campo, E. et al. *WHO Classification of Tumours of Haematopoietic and Lymphoid Tissues* (Lyon, 2017).
27. Cheson, B. D. et al. Recommendations for initial evaluation, staging, and response assessment of Hodgkin and non-Hodgkin lymphoma: the Lugano classification. *J. Clin. Oncol.* **32**, 3059–68 (2014).
28. Pitre-Champagnat, S. et al. Dynamic contrast-enhanced ultrasound parametric maps to evaluate intratumoral vascularization. *Invest. Radiol.* **50**, 212–217 (2015).

29. Park, A. Y. et al. A prospective study on the value of ultrasound microflow assessment to distinguish malignant from benign solid breast masses: Association between ultrasound parameters and histologic microvessel densities. *Korean J. Radiol.* **20**, 759–772 (2018).
30. Freeman, C. L. et al. Early progression after bendamustine-rituximab is associated with high risk of transformation in advanced stage follicular lymphoma. *Blood* **134**, 761–764 (2019).
31. Lin, Y., Xu, J. & Lan, H. Tumor-associated macrophages in tumor metastasis: biological roles and clinical therapeutic applications. *J. Hematol. Oncol.* **12**, 76 (2019).
32. Huang, Y. et al. Improving immune–vascular crosstalk for cancer immunotherapy. *Nat. Rev. Immunol.* **18**, 195–203 (2018).
33. Abe, Y. et al. A single-cell atlas of non-haematopoietic cells in human lymph nodes and lymphoma reveals a landscape of stromal remodeling. *Nat. Cell Biol.* **24**, 565–578 (2022).
34. Rumack, C. M. & Levine, D. *Diagnostic Ultrasound* (Elsevier Health Sciences, 2017).

Acknowledgements

Thanks for the support by the National Key Research and Development Program of China (2022YFC3400100 to YY.Z.), NSFC Key Project (82030050 to YY.Z.), National Natural Science Foundation of China (81801699 to RH. W.) for software development, design of the study, and Shanghai "Rising Stars of Medical Talents" Youth Development Program, Youth Medical Talents—Medical Imaging Practitioner Program to ZH.L. for data analysis and writing manuscript.

Author contributions

Conceptualization and Research Design: RH. W., ZH. L., WW. Z., and YY. Z; Methodology: RH. W., ZH. L., SQ. H., ZQ. W., and D. Z; Microcirculation Imaging Techniques: JP. Y. and MX. T; Data Collection and Analysis: ZX. Y., JQ. Z., X.X., and JN. H.; Writing-original draft RH. W. and ZH. L.; Writing-review and editing WL. Z., WW. Z, and YY. Z.; Supervision: MX. T., WW. Z., WL. Z., and YY. Z.

Declarations

Competing interests

The authors declare no competing interests.

Additional information

Supplementary Information The online version contains supplementary material available at https://doi.org/10.1038/s41598-025-01615-w.

Correspondence and requests for materials should be addressed to W.Z., Y.Z. or W.Z.